J Mater Sci: Mater Electron (2014) 25:1013–1016
DOI 10.1007/s10854-013-1680-6

Influence of the Eu^{3+} dosage concentration on luminescence properties of YPO_4:Eu^{3+} microspheres

Yan Lu · Huizhong Yu

Received: 16 November 2013 / Accepted: 13 December 2013 / Published online: 20 December 2013

Abstract In this study, YPO_4:Eu^{3+} microspheres with different Eu^{3+} dosage concentration were fabricated by a facile hydrothermal route at 200 °C for 10 h in the presence of citric acid. The YPO_4:Eu^{3+} samples were characterized by X-ray powder diffraction (XRD), transmission electron microscopy (TEM), scanning electron microscopy (SEM), and luminescence spectroscopy. The XRD results reveal that the YPO_4:Eu^{3+} samples presented a tetragonal structure. The TEM and SEM observations demonstrate that the YPO_4:Eu^{3+} samples with uniform sphere-like morphologies can be obtained at 200 °C for 10 h. The sizes of samples are in the range of 2–2.2 μm. The room temperature luminescence properties of YPO_4:Eu^{3+} samples were studied using an excitation wavelength of 227 nm. The emission spectrum displays the bands associated to the $^5D_0 \rightarrow {}^7F_J$ ($J = 1, 2$ and 4) electronic transitions characteristics of the Eu^{3+} cations at different positions. The influence of Eu^{3+} dosage concentration on luminescence properties of YPO_4:Eu^{3+} microspheres were studied carefully.

1 Introduction

Recently, more and more attentions have been focused on the study of the rare earth ions doped inorganic materials for application in luminescence materials [1]. The rare earth ions doped materials are the best phosphors for the generation of red, green, and blue colors in various applications [2]. Also, rare earth ions doped phosphors have some advantages when compared with other available luminescence materials (quantum dots or organic dyes), such as low toxicity, photostability, high thermal and chemical stability, high luminescence quantum yield (QY), and sharp emission bands [3]. Meanwhile, the luminescence properties can be tuned easily by adjusting the concentration of the rare earth ions [4]. Generally speaking, rare-earth doped orthophosphates, RPO_4 (R: Y, La, Gd, and Bi), have absorption edges at rather short wavelengths so that they are suitable for hosts of phosphors transparent in the wavelength region of the vacuum ultraviolet (VUV) [5–7]. For example, YPO_4 exhibits high thermal and chemical stability because Y^{3+} has an empty 4f electron shell with a stable structure [8]. It had been reported that YPO_4 is a good luminescence host for rare earth ions [9]. Furthermore, the YPO_4:Eu^{3+} phosphors are found to be one of the most familiar red emitting phosphors, and have been explored successfully for the design of luminescence devices [10].

It is well known that the intrinsic properties of inorganic materials are determined by their sizes, shapes, morphologies, compositions, and crystallinity [11]. The phosphor particles with spherical shape can offer the possibility of brighter cathodoluminescent performance, high definition, much improved screen packing and low scattering of light [12, 13]. In addition, spherical phosphor particles are able to increase the screen brightness and improve the resolution [14]. Therefore, YPO_4:Eu^{3+} phosphors with spherical morphology were synthesized by different methods [15, 16]. But there are hardly any reports about the influence of the Eu^{3+} dosage concentration on luminescence properties of YPO_4:Eu^{3+} microspheres. In the present work, Eu^{3+}-doped YPO_4 were synthesized by a surfactant-assisted approach. Especially, the influence of the Eu^{3+} dosage concentration on luminescence properties of YPO_4:Eu^{3+} microsphere was studied carefully.

Y. Lu (✉)
Department of Information and Engineering, Quzhou College of Technology, Quzhou 324000, China
e-mail: Lu_Yan09@126.com

H. Yu
Zhejiang Switchgear Factory Co., Ltd, Quzhou 324000, China

Table 1 YPO_4 samples with different Eu^{3+} dosage concentrations

Sample no.	Sample	Mole ratio of Y:Eu
1	$Eu_{0.01}Y_{0.99}PO_4$	0.99:0.01
2	$Eu_{0.02}Y_{0.98}PO_4$	0.98:0.02
3	$Eu_{0.03}Y_{0.97}PO_4$	0.97:0.03
4	$Eu_{0.04}Y_{0.96}PO_4$	0.96:0.04
5	$Eu_{0.05}Y_{0.95}PO_4$	0.95:0.05
6	$Eu_{0.06}Y_{0.94}PO_4$	0.94:0.06
7	$Eu_{0.07}Y_{0.93}PO_4$	0.93:0.07

2 Experimental

All the chemical reagents were of analytical grade and used as received without further purification. All chemical reagents were obtained from Nanjing Chemical Reagent Co., Ltd, China. Experimental details include following steps. Firstly, 2.5 mmol of $Ln(NO_3)_3$ (Ln = Y and Eu, with different mole ratios of Y:Eu) was dissolved in 15 ml of deionized water (Table 1), and then 0.10 g of citric acid ($C_6H_8O_7$) was introduced into the solution. Secondly, 2.5 mmol of $(NH_4)_2HPO_4$ was dissolved in 15 mL of deionized water, too. Thirdly, the $(NH_4)_2HPO_4$ solution was added drop-wise into the $Ln(NO_3)_3$ solution under vigorous stirring, until a white-colored solution was obtained. Finally, the resulting suspension was transferred into a 40 ml Teflon-lined stainless steel autoclave with a filling capacity of 75 % and maintained at 200 °C for 10 h. After the hydrothermal system was cooled to room temperature naturally, the precipitates were collected, washed several times with distilled water and dried in air at 80 °C for 8 h.

The X-ray diffraction (XRD) patterns of the samples were examined using a Japan RigaKu D/max-g X-ray diffractometer system with graphite monochromatized Cu Kα irradiation (λ = 1.5418 Å). The transmission electron microscopy (TEM) was taken using a JEM-100CX TEM running at an accelerating voltage of 100 kV. The scanning electron microscopy (SEM) images were taken on a JEOL JSM-6700F scanning electron microscope. The excitation and emission spectra of the samples were measured by an Edinburgh FLS920 fluorescence-lifetime and steady-state spectrometer. All the measurements were taken at room temperature.

3 Results and discussions

Figure 1 shows the XRD patterns of the as-obtained $Eu_{0.05}Y_{0.95}PO_4$ samples. It reveals that all the diffraction peaks can be indexed to tetragonal structured YPO_4 readily according to JCPDS-840335. No obvious impurity phase is found in the samples. The XRD patterns are similar for YPO_4:Eu^{3+} samples with different Eu^{3+} dosage concentrations.

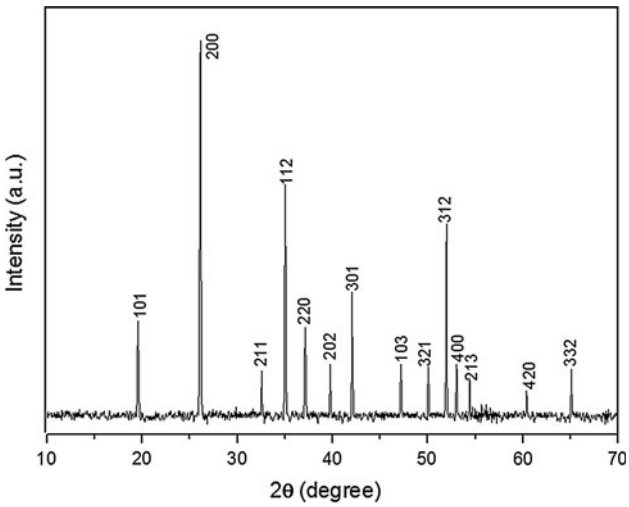

Fig. 1 XRD pattern of $Eu_{0.05}Y_{0.95}PO_4$ microspheres

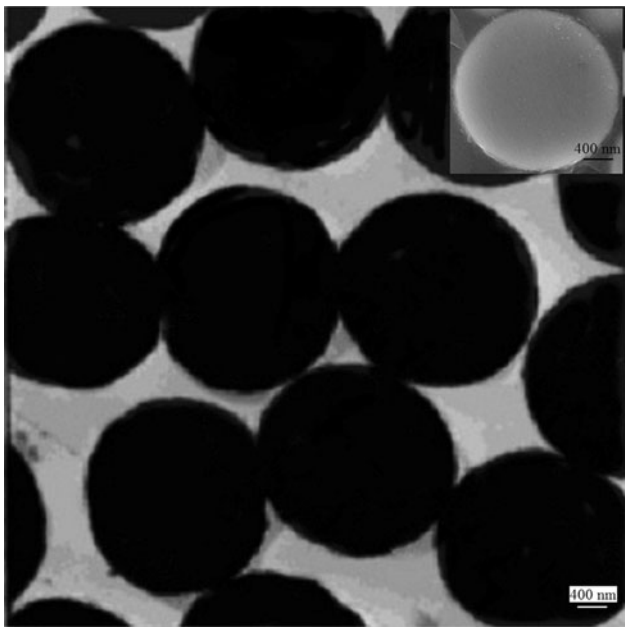

Fig. 2 TEM and SEM of $Eu_{0.05}Y_{0.95}PO_4$ microspheres

The SEM and TEM images of the $Eu_{0.05}Y_{0.95}PO_4$ samples are shown in Fig. 2. From Fig. 2, one can see that the formation of a large quantity of spherical particles in micrometer scale. The sizes of $Eu_{0.05}Y_{0.95}PO_4$ microspheres are in the range of 2–2.2 μm. A SEM micrograph of $Eu_{0.05}Y_{0.95}PO_4$ particles shown in the inset of Fig. 2 reveals that spherical particles have smooth surface. The morphologies are similar for YPO_4:Eu^{3+} samples with different Eu^{3+} dosage concentrations.

Figure 3 displays the excitation and emission spectra of the $Eu_{0.05}Y_{0.95}PO_4$ microspheres. The excitation spectrum consists of a strong band centered at 227 nm and a band centered at 397 nm. The strong band centered at 227 nm is due to the

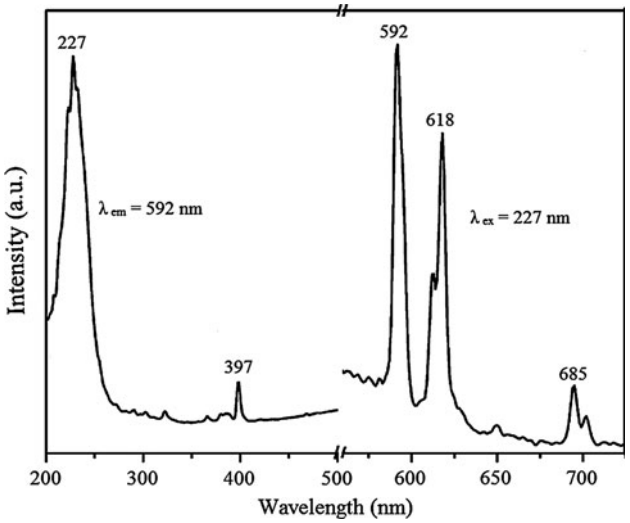

Fig. 3 Excitation and emission spectra of $Eu_{0.05}Y_{0.95}PO_4$ microspheres

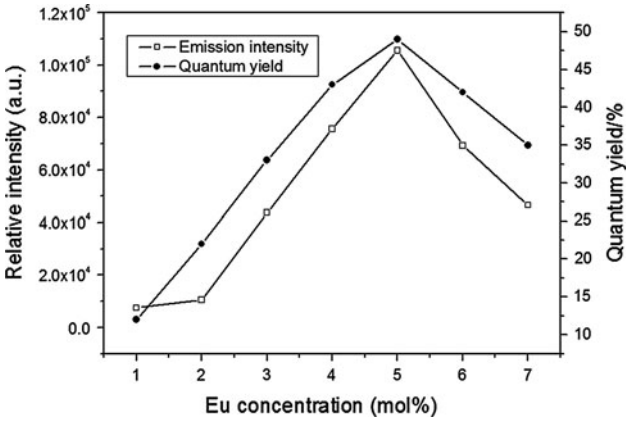

Fig. 4 Emission intensities and quantum yield values of samples with different Eu^{3+} dosage concentration

oxygen-to-europium charge transfer band (CTB) [17]. The band centered at 397 nm is attributed to the $^7F_0 \rightarrow {}^5L_6$ transition of the Eu^{3+} ions. The emission spectrum is monitored at the most intense Eu^{3+} emission wavelength. As observed, it consists of several sharp lines due to the direct emission of the Eu^{3+} cations from the ground state to higher levels of the 4f-manifold. The emission spectrum displays the bands associated to the $^5D_0 \rightarrow {}^7F_J$ (J = 1, 2 and 4) electronic transitions characteristics of the Eu^{3+} cations at different positions. Among them, the $^5D_0 \rightarrow {}^7F_1$ transitions are the strongest and characterized by an orange–red emission. The $^5D_0 \rightarrow {}^7F_1$ lines originate from the magnetic dipole transition, while the $^5D_0 \rightarrow {}^7F_2$ lines originate from the electric dipole transition [18]. The electric dipole transition is allowed only on the condition that the Eu^{3+} ion occupies a site without an inversion center and is sensitive to local symmetry, which induces the relatively strong of $^5D_0 \rightarrow {}^7F_1$ transition and the relatively weak of $^5D_0 \rightarrow {}^7F_2$ transition. In the emission spectrum of the $Eu_{0.05}Y_{0.95}PO_4$ microspheres, the most peak centered at 592 nm ($^5D_0 \rightarrow {}^7F_1$), which is stronger than that of the 618 nm ($^5D_0 \rightarrow {}^7F_2$), suggesting a higher occupancy of Eu^{3+} in the asymmetric environment. The excitation and emission spectra are similar for YPO_4:Eu^{3+} samples with different Eu^{3+} dosage concentrations, besides the different emission intensities.

Figure 4 shows the Eu^{3+} emission intensities of ($^5D_0 \rightarrow {}^7F_1$) transition and QY values for all of samples as a function of Eu^{3+} dosage concentration. It can be seen that the emission intensities of samples increase with the increases of Eu^{3+} dosage concentration and reach a maximum value around 5 mol % Eu^{3+}. Firstly, increases of Eu^{3+} dosage concentration decrease the degree of symmetry in the samples because of the bigger radius of Eu^{3+}. Lower symmetry will lead to higher emission intensity. Secondly, the distance of Eu^{3+} decreases with the increases of Eu^{3+} dosage concentration, which enhances the interaction of Eu^{3+}. The decreases of the distance between the luminescence centers will cause the probability of nonradiative energy migration between Eu^{3+} ions and lead to nonradiative deexcitation, which is known as the concentration quenching. The experimental Eu^{3+} dosage concentration in YPO_4 of concentration quenching is 5 mol %. The QY value also continues to increase with the increase of Eu^{3+} concentration up to 5 mol %, where a maximum QY value of 0.49 is acquired. This is in good agreement with the tendency observed in emission intensity.

The decay process of YPO_4:Eu^{3+} phosphors with different Eu^{3+} dosage concentration are investigated and shown in Fig. 5. All the curves can be well fit into a single-exponential function as $I(t) = I_0 \exp(-t/\tau_1)$ (I_0 is the initial emission intensity at $t = 0$ and τ is the 1/e lifetime of the emission center). The average lifetime values are calculated from the decay curves and shown in Fig. 5, too. The lifetime value is found to be maximal (3.15 ms) for $Eu_{0.05}Y_{0.95}PO_4$ sample, which is in accordance with the emission intensities corresponding to the samples shown in Fig. 4. This phenomenon is owing to the fact that the material with long lifetime of the emission transitions would create strong population inversion upon excitation, and hence it would cause high excited state electrons and thereby enhancing the rate of recombination. Therefore, it produces strong fluorescence [19]. With an increase in Eu^{3+} dosage concentration, the extent of energy transfer from host to Eu^{3+} increases as there are a number of Eu^{3+} ions in the lattice to receive energy from the host. This effect will lead to an increase in emission intensities from Eu^{3+} ions. Hence, the lifetime values of the samples increase with the increases of Eu^{3+} dosage concentration up to 5 mol %, because of the domination of the host to Eu^{3+} energy transfer effect. However, there are interactions among Eu^{3+} ions. The extent of Eu^{3+}–Eu^{3+} interaction increases due to the reduced Eu^{3+}–Eu^{3+} internuclear distances and this leads to energy transfer among different Eu^{3+} ion followed by

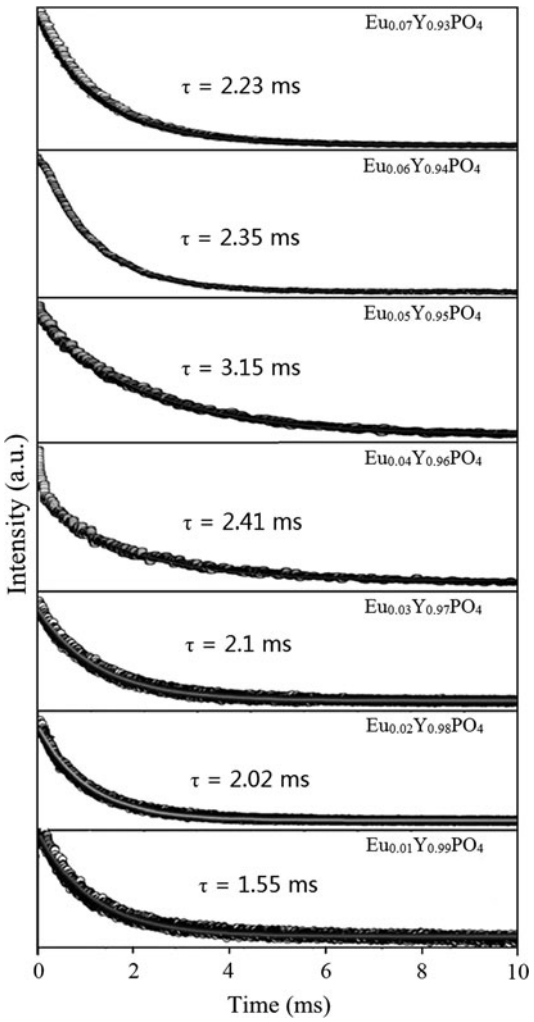

Fig. 5 Decay curves of samples with different Eu^{3+} dosage concentration

nonradiative decay of the excited state. Such interactions result in a decrease in the excited state lifetime corresponding to Eu^{3+} ions. Therefore, the lifetime values of the samples decrease when the Eu^{3+} dosage concentration is more than 5 mol %, because of the domination of the Eu^{3+}–Eu^{3+} interaction. In other words, the lifetime is determined by two competing and opposite effects, namely an increase in Eu^{3+}–Eu^{3+} interaction and an increase in the extent of energy transfer from host to Eu^{3+} ions.

4 Conclusions

YPO_4:Eu^{3+} microspheres with different Eu^{3+} dosage concentration were synthesized at temperature of 200 °C. The size of microspheres is in the range of 2–2.2 μm. The emission spectrum of samples displays the bands associated to the $^5D_0 \rightarrow {}^7F_J$ (J = 1, 2 and 4) electronic transitions characteristics of the Eu^{3+} cations at a position. It is found that the concentration has an obvious influence on emission intensities, QYs and lifetimes of samples. The emission intensity and the lifetime are determined by two competing and opposite effects, namely an increase in Eu^{3+}–Eu^{3+} interaction and an increase in the extent of energy transfer from host to Eu^{3+} ions. The $Eu_{0.05}Y_{0.95}PO_4$ sample has the highest value of emission intensity, quantum yield and lifetime.

Acknowledgments This work is supported financially by the Quzhou Municipal Science and Technology Project (Grant No. 2013Y018), and the Natural Science Foundation of Zhejiang Province (Grant No. Y1110557).

References

1. Y. Zhang, H. He, X. Yang, A. Zheng, Y. Fan, Powder Technol. **224**, 175 (2012)
2. G. Blass, B.C. Grabmaier, *Luminescent materials* (Springer, Berlin, 1994)
3. S. Rodriguez-Liviano, F.J. Aparicio, T.C. Rojas, A.B. Hungría, L.E. Chinchilla, M. Ocana, Cryst. Growth Des. **12**, 635 (2012)
4. U. Rambabu, D.P. Amalnerkar, B.B. Kale, S. Buddhudu, Mater. Res. Bull. **35**, 929 (2000)
5. K. Park, M.H. Heo, K.Y. Kim, S.J. Dhoble, Y. Kim, J.Y. Kim, Powder Technol. **237**, 102 (2013)
6. S. Lin, X. Dong, R. Jia, Y. Yuan, J. Mater. Sci.: Mater. Electron. **21**, 38 (2010)
7. S. Liu, W. Zhang, Z. Hu, Z. Feng, X. Sheng, Y. Liang, J. Mater. Sci.: Mater. Electron. **24**, 4253 (2013)
8. H. Lai, A. Bao, Y.M. Yang, Y.C. Tao, H. Yang, Y. Zhang, L.L. Han, J. Phys. Chem. C **112**, 282 (2008)
9. E. Nakazawa, Chem. Phys. Lett. **56**, 161 (1978)
10. O. Guillot-Noël, B. Viana, B. Bellamy, D. Gourier, G.B. Zogo-Mboulou, S. Jandl, Opt. Mater. **13**, 427 (2000)
11. S. Mann, G.A. Ozin, Nature **382**, 313 (1996)
12. M.I. Martinez-Rubio, T.G. Ireland, G.R. Fern, J. Silver, M.J. Snowden, Langmuir **17**, 7145 (2001)
13. G. Wakefield, E. Holland, P.J. Dobson, J.L. Hutchison, Adv. Mater. **13**, 1557 (2001)
14. H. Wang, C.K. Lin, X.M. Liu, J. Lin, M. Yu, Appl. Phys. Lett. **87**, 181907 (2005)
15. M. Yang, H. You, N. Guo, Y. Huang, Y. Zheng, H. Zhang, Cryst. Eng. Comm. **12**, 4141 (2010)
16. L. Zhang, G. Jia, H. You, K. Liu, M. Yang, Y. Song, Y. Zheng, Y. Huang, N. Guo, H. Zhang, Inorg. Chem. **49**, 3305 (2010)
17. L. Yu, H. Song, S. Lu, Z. Liu, L. Yang, X. Kong, J. Phys. Chem. B **108**, 16697 (2004)
18. B.R. Judd, Phys. Rev. **127**, 750 (1962)
19. S. Buddhudu, C.H. Kam, S.L. Ng, Y.L. Lam, B.S. Ooi, Y. Zhou, K.S. Wong, Mater. Sci. Eng., B **72**, 27 (2000)